Corrosion Science 178 (2021) 109053

Contents lists available at ScienceDirect

Corrosion Science

journal homepage: www.elsevier.com/locate/corsci

Crevice corrosion of solution annealed 25Cr duplex stainless steels: Effect of W on critical temperatures

Cristian Torres [a,*], Roy Johnsen [a], Mariano Iannuzzi [a,b]

[a] Department of Mechanical and Industrial Engineering, Norwegian University of Science and Technology, Richard Birkelands veg 2b, 7491, Trondheim, Norway
[b] Curtin Corrosion Centre, Curtin University, GPO Box U1987, Perth, WA, 6845, Australia

ARTICLE INFO

Keywords:
A. Tungsten
A. Duplex stainless steel
B. PD-GS-PD
C. Crevice corrosion
C. Repassivation potential

ABSTRACT

In this work, the influence of tungsten on the crevice corrosion resistance of three super duplex stainless steels (SDSS) containing 0.0, 0.6, and 2.1 wt.% W was determined. The PD-GS-PD technique was used to estimate the critical crevice repassivation temperature by performing tests at different temperatures. Additionally, long-term potentiostatic experiments were conducted as a function of temperature in natural seawater to validate PD-GS-PD testing. Results showed that W improved crevice corrosion resistance as evidenced by the higher initiation and repassivation crevice temperatures, which were 7.5–15 °C higher in the 2.1 wt.% W SDSS than in the W-free case.

1. Introduction

In the case of super duplex stainless steels (SDSS), it is known that increasing the Cr, Mo, and N content improves their localised corrosion resistance to chloride-containing electrolytes with a pH value ranging from slightly acidic to moderately alkaline [1–6]. Tungsten has also been shown to improve the localised corrosion resistance of SDSS, although the mechanisms and the extent to which W can improve pitting and crevice corrosion performance are still a cause of debate within the scientific community [7,8].

Two different roles of W need to be considered when investigating its effect on corrosion resistance: (i) its influence as a solid solution element in the solution annealed (SA) condition; and (ii) its impact on the precipitation kinetics of deleterious phases in, e.g., isothermally aged materials. The scope of this work focuses on the former role, as the W effect on precipitation kinetics has been addressed elsewhere [8].

Literature published so far on SA stainless steel indicates that pure W does not form a passive layer [9]. However, there is disagreement as to whether W contributes to passivity when it is added to Fe-Cr stainless steels. Belfrouh et al. [10] reported a detrimental effect of W when added to austenitic stainless steels in the absence of Mo; however, the authors indicated that when combined with Mo, W could improve pitting corrosion resistance. In contrast, Bui et al. [9] performed potentiodynamic polarisations of austenitic stainless steels as a function of W content in acid and neutral chloride-containing-electrolytes. In some conditions, the authors included tungstates to study the inhibition effect of W both as a solid solution element and as an anodic inhibitor in the electrolyte. The results showed a clear improvement in the corrosion resistance of the material with increasing W content, and, according to the authors, W was present in the passive layer in the form of WO_3. The influence of W on improving passivity was a function of the pH of the bulk electrolyte. In acid media, W interacted with water to form insoluble WO_3. In neutral pH, WO_3 bonded to the substrate, increasing the stability of the passive film. The tungstates added to the electrolyte inhibited corrosion by surface absorption without electrochemical reduction on the passive layer. Tomashov et al. [11] studied the

Abbreviations: CCT, critical crevice temperature; CPP, cyclic potentiodynamic polarisation; CPT, critical pitting temperature; CRA, corrosion-resistant alloy; E_{corr}, corrosion potential; E_P, pitting potential; E_R, repassivation potential; $E_{R,Crev}$, crevice repassivation potential; E_{Trans}, transpassive potential; EDS, energy-dispersive x-ray spectroscopy; GS, galvanostatic polarisation; ICP-MS, inductively coupled plasma mass spectrometry; IFM, infinite focus microscope; i_{GS}, current density of galvanostatic polarisation step; i_{pass}, passive current density; OCP, open circuit potential; PD, potentiodynamic polarisation; PD-GS-PD, potentiodynamic-galvanostatic-potentiodynamic; PRE_N, pitting resistance equivalent considering the N content; $PRE_{N,W}$, pitting resistance equivalent considering the N and W content; PS, potentiostatic polarisation; PTFE, polytetrafluoroethylene; Q, electric charge; Q_{exp}, experimental electric charge; SA, solution annealed; SEM, scanning electron microscope; SDSS, super duplex stainless steel; THE, Tsujikawa-Hisamatsu electrochemical; T_R, repassivation temperature; $T_{R,Crev}$, crevice repassivation temperature; α, ferrite; γ, austenite.

* Corresponding author.
E-mail address: cristian.torres@ntnu.no (C. Torres).

https://doi.org/10.1016/j.corsci.2020.109053
Received 4 June 2020; Received in revised form 31 August 2020; Accepted 29 September 2020
Available online 10 October 2020

influence of W additions from 0.18 to 2.67 wt.% to austenitic stainless steels. The authors obtained lower corrosion rates and higher pitting potentials (E_P) as the W content increased. However, the 0.18 wt.% W addition worsen the corrosion resistance when compared with the W-free base alloy.

For ferritic stainless steels, Ahn et al. [12] obtained a clear improvement in pitting corrosion resistance in neutral and acid chloride-containing electrolytes. W had the same beneficial effect as Mo when added at the same at.% (i.e., half the quantity of Mo in wt.%). However, the authors reported no synergistic effects when both elements were added together. Cho et al. [13] also studied ferritic stainless steels, analysing the influence of W on the repassivation kinetics. The authors observed a beneficial effect of W on the localised corrosion resistance of the materials, although an equal addition of Mo (in wt.%) had 1.6 times the effect of W, i.e., W and Mo would have had approximately the same beneficial influence if added at the same at.%. Goetz et al. [14] observed enrichment of Mo and W at the surface of ferritic stainless steels. However, the improvement in localised corrosion resistance was not attributed to this enrichment, but to a lower activity of Fe. The authors concluded that Mo had a higher beneficial effect than W, even at equal at.% additions.

Habazaki et al. [15] investigated additions of Mo and W to amorphous Fe-Cr alloys. Both elements, although W to a greater extent, improved corrosion resistance of the materials by inhibiting Cr dissolution during passivity. Thereby, the passive layer was enriched in Cr and localised corrosion was averted. Nevertheless, when the W and Mo were added in excess (10 at.%), the dissolution during passivation increased and the inhibiting effect was lost. Consequently, the results in the literature seem to indicate the existence of an optimal W concentration range within which W improves the stability of the passive film. W might be detrimental or ineffective outside this range; nevertheless, the optimal composition range is not well defined.

Despite the extent of the research presented above, all these investigations focused on single-phase stainless steels (either austenitic or ferritic) or amorphous alloys. Consequently, there is a lack of knowledge on the role of W on highly allowed dual-phase stainless steels such as duplex stainless steels. Recently, Haugan et al. [7] compared two different SDSS containing W, specifically 0.55 wt.% and 2.2 wt.%. The authors performed different electrochemical techniques to obtain the critical pitting temperature (CPT), the critical crevice temperature (CCT) and the repassivation temperature (T_R); the later one determined based on repassivation potentials (E_R) measured following ASTM G61 [16]. Although the authors found a marked improvement in crevice corrosion resistance with W content; a reference W-free alloy was not included in the test matrix, and the samples were extracted from components made using different forming methods (i.e., extruded pipe vs. rolled plate). Additionally, the cyclic potentiodynamic polarization (CPP) technique adapted from ASTM G61 has limitations that need to be considered when studying highly alloyed stainless steels.

1.1. Electrochemical techniques to determine crevice corrosion resistance

E_R and, for studies using crevice formers, $E_{R,Crev}$ are often obtained by means of potentiodynamic tests. ASTM G61 describes the CPP technique, which is the most widely used. The CPP technique consists of a slow potentiodynamic polarisation (PD) scan to a pre-specified current density value. The current density value must be high enough to initiate localised corrosion in the forward scan. As soon as this current density value is reached, the direction of the polarisation is reverted during the backward PD. E_R is then defined as either a cross-over potential or when the backward scan reaches the passive current density (i_{pass}) [17]. However, several studies [18–21] have indicated the dependence of E_R with the extent of pit and crevice propagation, which can be related to the electrical charge (Q) passed during the forward scan. For certain stainless steels and corrosion resistant alloys (CRAs), i.e., UNS S30400, S31603 and N08825, only when the propagation was deep enough (i.e., $Q > 10-30$ C/cm^2), E_R became independent of the size of the attack [21–25]. These findings imply the existence of a minimum pit or crevice depth to obtain reproducible E_R values. Especially for highly alloyed CRAs, the CPP method might allow insufficient time for localised corrosion propagation during the forward step, as the backward potentiodynamic scan starts as soon as the pre-defined current density is reached. Additionally, several investigations [23,26] have shown an inherent large scatter in critical potentials since the extent of the localised corrosion attack might be insufficient to ensure a lower-bound E_R value.

Researchers have, thus, developed alternative methods to circumvent the limitations of the CPP technique. Tsujikawa and Hisamatsu [27] developed a new electrochemical test to study crevice corrosion of nickel-based CRAs, which is referred to as the Tsujikawa-Hisamatsu Electrochemical (THE) test. This multi-step technique is now standardised in the ASTM G192 standard and consists of the following steps [28]: (i) PD to a potential more positive than critical potential, (ii) galvanostatic polarisation (GS) for 2 h to let localised corrosion propagate, and (iii) iterative potentiostatic polarisation (PS), lowering the potential 10 mV every 2 h until repassivation is achieved. Thanks to the GS step, the total charge passed is better controlled as the current is held constant during the time of the galvanostatic step. As a result, a sufficiently deep localised attack can develop, which leads to more reproducible E_R values [21–24]. E_R is defined in this technique as the highest potential where the current stops increasing during the PS. Nevertheless, the THE method is slow and time consuming as E_R is normally found at low potentials. Thus, it often takes many iterations and a long time to reach E_R using 10 mV steps every 2 h. Additionally, in some cases [29], it was difficult to discern when repassivation occurred due to the current behaviour during the PS step, complicating the determination of E_R.

Consequently, Mishra and Frankel [29] changed the third step of the THE test to a backward PD scan. As in the case of CPP, E_R is defined as the cross-over of both potentiodynamic scans or when the backward scan reaches i_{pass}. This technique was referred to as the PD-GS-PD method by the authors, named to reflect the three different steps, specifically: (i) potentiodynamic polarisation scan (PD), (ii) galvanostatic polarisation (GS), and (iii) reverse potentiodynamic polarisation scan (PD). Thereby, the issues mentioned above with the CPP and the THE techniques were resolved. In a PD-GS-PD scan, crevice corrosion develops during the GS step, resulting in a low scatter of the results while keeping the testing time short.

The PD-GS-PD has successfully been used to analyse the localised corrosion resistance of nickel-based alloys [29–35]. The PD-GS-PD technique has, as well, been used to test conventional [24] and highly-alloyed stainless steels, specifically UNS S32205 and S32750 [36,37]. Results showed that the PD-GS-PD method gave the most conservative crevice repassivation potentials ($E_{R,Crev}$) values among the different methods, i.e., the lowest values in comparison to the CPP and THE tests [29–31]. In addition, these E_R values were independent of the scan rate used during the PD steps [29], torque applied to the crevice former (if greater than 2 N·m) [31], and the charge passed during the GS step [30]. These results indicated that the PD-GS-PD technique allowed sufficient localised attack propagation during the GS step to let E_R become independent of the experimental variables mentioned above. The PD-GS-PD method is, thus, a proven technique for testing localised corrosion resistant of highly alloyed CRAs, such as SDSS.

Since E_R is used to determine the localised corrosion resistance of an alloy, it can be used to analyse the role of different alloying elements on the resulting corrosion resistance [32,33]. Additionally, by testing at different temperatures, the PD-GS-PD technique can be used to determine the critical crevice temperature as well as the crevice repassivation temperature ($T_{R,Crev}$) [7,38].

The objective of this investigation was to quantify the crevice corrosion resistance of commercial SDSS as a function of W content. Therefore, three SA materials differing mainly in their W content were compared. Firstly, PD-GS-PD tests were conducted at incremental

temperatures to determine changes in $T_{R,Crev}$ as a function of W content. The results were, then, validated using long-term potentiostatic testing in natural seawater.

2. Experimental

Three different materials were employed in this work, i.e., UNS S32750, S32760, and S39274. Table 1 shows their chemical composition. UNS S32750, a W-free SDSS, was used as a reference material; whereas UNS S32760 and S39274 contained 0.6 wt.% W and 2.1 wt.% W, respectively. All materials were received as extruded pipes with a 30 mm wall thickness and a 203.2 mm diameter. Additionally, a 100 mm by 150 mm by 9.5 mm UNS S39274 rolled plate was included in the test program to compare the results to Haugan et al. [7] and analyse the influence of product form variations.

Round samples with a thickness of 3 mm were machined from all materials. The final diameter for UNS S32750 and S32760 specimens was 25 mm, whereas the diameter of the UNS S39274 specimens was 30 mm.

2.1. Sample preparation

Both extruded pipe and rolled plate UNS S39274 samples were received in the SA condition (heat-treated at 1085 °C for 10 min). On the other hand, UNS S32750 and UNS S32760 were received as extruded and, thus, were solution annealed according to the manufacturer's specifications in an air furnaced at 1100 °C for 15 min and rapidly quenched in water. Fig. 1 includes micrographs of the four materials studied in this work. All materials were within the acceptable austenite/ferrite ratio range [7,8], i.e., 40–60 %.

The specimens were subsequently wet ground down to 500 US-grit SiC paper, rinsed with acetone, followed by distilled water and ethanol, and cleaned in an ultrasonic bath with ethanol for 5 min.

The coupons were mounted in the multi-crevice assembly shown in Fig. 2 as described in ISO18070 [39]. The crevice washers were made of polytetrafluoroethylene (PTFE) with 12 artificial crevice slots (i.e., 24 in total). The washers were covered with PTFE tape as indicated by ASTM G192, which improved the reproducibility of the results as determined by preliminary testing [28]. The applied torque was 5 N·m [37]. A small hole of 2 mm in diameter was drilled close to the edge of each specimen to pass a 200 μm Pt wire, which was used to suspend the multi-crevice assembly as illustrated elsewhere [40–43].

The total surface area of the specimens exposed to the electrolyte was approximately 6.5 cm^2 for UNS S32750 and S32760, and 11 cm^2 for S39274. The area covered by the crevice former was 4.9 cm^2 for all specimens.

2.2. Crevice corrosion tests in 3.5 wt% NaCl

The experiments were carried out in a double-wall cell filled with approximately 160 mL of 3.5 wt.% NaCl, pH 6.5 solution (a minimum volume/specimen area ratio of 14.5 cm^3/cm^2 for UNS S39274, which had the largest total surface area). The electrolyte was purged with N_2 for 2 h before the sample was immersed. The cell was continuously purged for the duration of the tests. The dissolved oxygen concentration, which was monitored during testing by means of a fibre optic oxygen meter, remained below 10 ppb from the moment the sample was immersed and until the end of the experiment.

The electrochemical tests were performed at different temperatures: room temperature (22 ± 1 °C), 40 °C, 50 °C, and 60 °C. The temperature was controlled by a water bath connected to the jacketed cell, except for the room temperature tests that were performed at the pre-set laboratory temperature. A condenser filled with continuously running cold tap water (approximately 10 °C) was placed in the outlet of the gas port to avoid evaporation of the electrolyte during testing.

The PD-GS-PD tests were conducted in a conventional three-electrode setup. An Ag/AgCl KCl saturated electrode was used as the reference electrode and a Pt mesh as the counter electrode. All samples were freely exposed at the corrosion potential (E_{corr}) for 15 min after immersion and before polarisation. Subsequently, a small cathodic current density of 1 μA/cm^2 was applied to remove possible surface contamination [37]; followed by another 30 min of E_{corr} exposure to allow the surface to stabilise.

The following procedure for the PD-GS-PD technique was used [37]: (i) the PD step was conducted at a scan rate of 0.167 mV/s, starting 30 mV below E_{corr} and ending when a pre-defined current density (i_{GS}) was reached, (ii) the GS step was done at the pre-defined i_{GS} for 2 h, and (iii) the reverse PD step was done at a scan rate of 0.167 mV/s, starting at the last potential measured during GS and ending when repassivation was achieved. $E_{R,Crev}$ was defined in two different ways for comparison: (i) as the cross-over potential of the forward and backward PD scans, and (ii) as the potential at which i_{pass} reached 1 μA/cm^2 [17]. The i_{GS} values were: (i) 25 μA/cm^2 for all temperatures [37], and (ii) 100 μA/cm^2 for 50 °C and 60 °C. The highest current density, 100 μA/cm^2, was high enough to avoid metastable activity and current noise triggering the start of the following step in the PD-GS-PD technique, as explained below.

Once the $E_{R,Crev}$ was obtained for each material at each different temperature, the $T_{R,Crev}$ was defined as the temperature at which the $E_{R,Crev}$ experienced a sharp drop from potentials associated with transpassivity to lower, usually negative, potentials [7,44].

All tests were conducted at least in duplicated, while additional experiments were conducted as needed when large variations in $E_{R,Crev}$ were found to confirm the repeatability of the results [23,26]. In this regard, the number of tests conducted at temperatures in the vicinity of $T_{R,Crev}$ was up to 8 per condition.

2.3. Long-term experiments in natural seawater

UNS S32750 and UNS S39274 extruded pipe specimens were exposed in natural seawater with the same crevice assembly as described in section 2.1. The seawater was taken from the Trondheim fjord (Norway) from 80 m depth and brought into a 5 L glass container with an inlet close to the bottom and an outlet close to the top to let the natural seawater flow continuously during the test. The container was placed on top of a hot plate. The temperature was regulated using a PID controller connected to a thermocouple placed close to the specimens. The set temperature was maintained within a ±1 °C variation. The seawater flow was approximately 4 mL/min to avoid turbulence while ensuring a uniform temperature within the container.

Table 1
Chemical composition in wt.%.

Material (UNS)	PRE_N*/ $PRE_{N,W}$**	Si	Mn	Cu	Ni	Cr	Mo	N	W	Fe
S32750	43 / 43	0.27	0.51	0.14	6.42	**25.6**	**3.83**	**0.30**	–	62.9
S32760	41 / 42	0.50	0.60	0.60	7.1	**25.2**	**3.6**	**0.25**	**0.62**	61.5
S39274 extruded pipe	40 / 43	0.24	0.71	0.52	6.3	**24.9**	**3.1**	**0.29**	**2.1**	61.8
S39274 rolled plate	40 / 43	0.20	0.71	0.48	7.6	**24.6**	**2.9**	**0.35**	**2.1**	61.1

*PRE_N = %Cr + 3.3 %Mo + 16 %N.
**$PRE_{N,W}$ = %Cr + 3.3 (%Mo + 0.5 %W) + 16 %N.

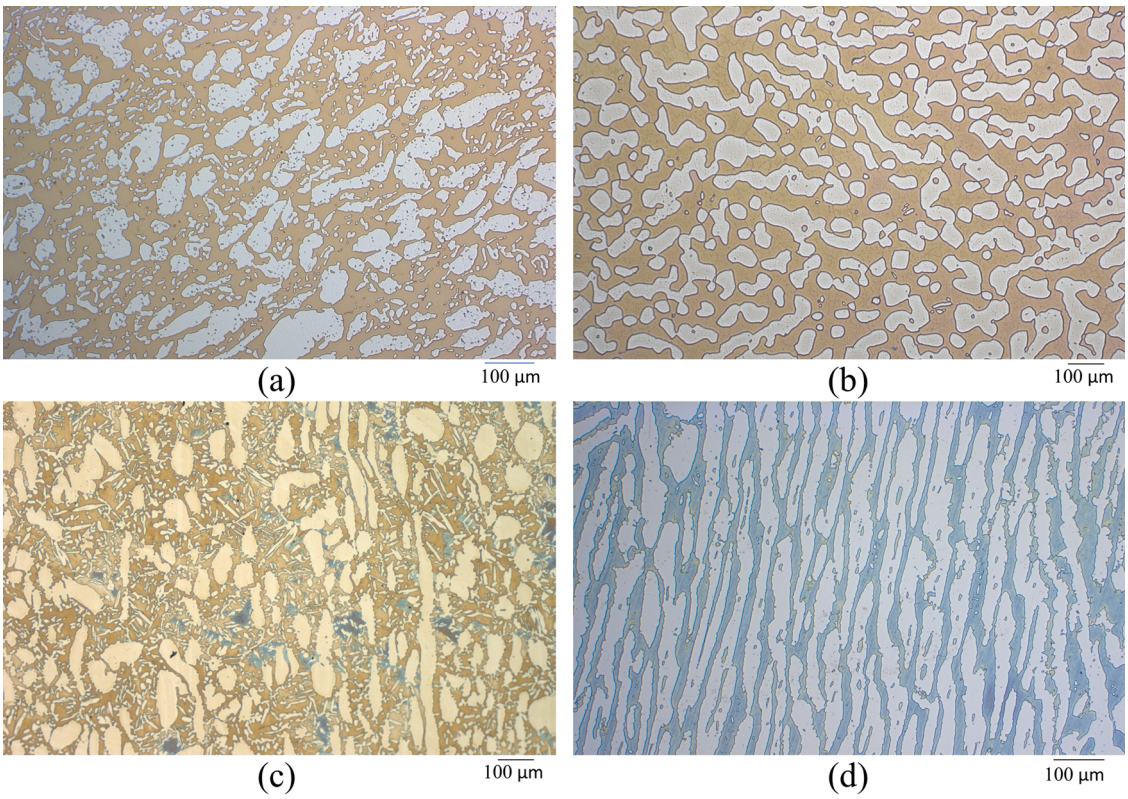

Fig. 1. Light optical micrographs of (a) UNS S32750, (b) UNS S32760, (c) UNS S39274 extruded pipe, and (d) UNS S39274 rolled plate. The microstructure was revealed by applying two different etching steps. In the first step, a 15 wt.% KOH solution was used, and a potential of 3 V was applied for 12 s. In the second step, the solution was 20 wt.% NaOH with an applied potential of 1.5 V for 10 s.

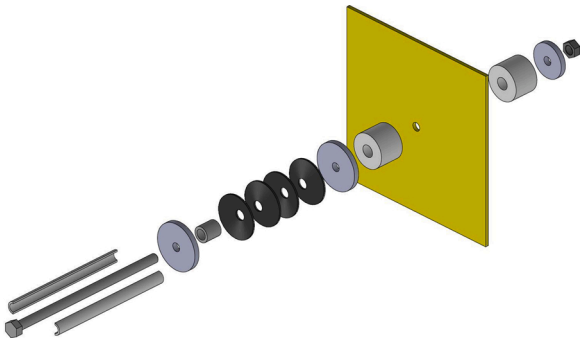

Fig. 2. Schematic diagram of the multi-crevice assembly described in ISO18070 [39].

The specimens were exposed at: (i) open circuit potential (OCP), and (ii) polarised at +600 $mV_{Ag/AgCl}$, to simulate chlorinated seawater [7, 40]. An Ag/AgCl KCl saturated reference electrode was used, and in the case of the polarised samples, a Pt mesh served as the counter electrode. The tests with the specimens at OCP started at 50 °C and the temperature was increased fortnightly at 5 °C steps until crevice corrosion initiated. The initiation of crevice corrosion was determined as a sharp drop on the OCP as described by Oldfield and Sutton [45]. For the specimens polarised to +600 $mV_{Ag/AgCl}$, the initial temperature was 40 °C and was increased in 5 °C steps weekly. Crevice corrosion initiation was assumed when the current density exceeded 25 µA/cm^2 for over 24 h. The temperature at which crevice corrosion initiated was considered the CCT. After crevice initiation, the specimens were kept at that temperature for at least 48 h before decreasing the temperature at 2.5 °C steps every 48 h until (i) the OCP value recovered for the freely exposed samples, or (ii) the current decreased below 25 µA/cm^2 for over 24 h for the polarised samples . This temperature was considered the $T_{R,Crev}$. Two specimens of the same material were exposed in the same container simultaneously for repeatability. Since the replicated polarized specimens were connected to the same potentiostat, the temperature scan was reversed once both samples showed crevice corrosion.

2.4. Characterisation

After testing, the specimens were analysed by means of an Infinite Focus Microscope (IFM) employed as optical microscope with the possibility of taking 3D pictures of the surface. The number of crevice attacks present on both sides of the specimens were identified and their depth measured. The volume and projected area on the surface of the crevices were calculated using a commercial surface and image analysis software (MountainMaps) [46]. In selected cases, the corrosion attack was further analysed in a scanning electron microscope (SEM) coupled with energy-dispersive x-ray spectroscopy (EDS).

At the end of the PD-GS-PD tests, the electrolyte was stored in plastic containers and brought to the Department of Chemistry at the Norwegian University of Science and Technology (NTNU) where the concentration of released ions in the solution were measured by Inductively Coupled Plasma Mass Spectrometry (ICP-MS).

The total Q measured during the PD-GS-PD tests (Q_{exp}) was calculated as well from the GS and reverse PD steps until repassivation was achieved, assuming that the Q provided by the forward PD was negligible due to the low current densities measured and the short time of this step compared to the rest of the test.

3. Results

3.1. Critical crevice temperatures by the PD-GS-PD technique

Fig. 3 illustrates two results obtained with the PD-GS-PD technique. In the case of Fig. 3a, the specimen suffered crevice corrosion, indicated by a large hysteresis loop and a low $E_{R,Crev}$. In contrast, Fig. 3b illustrates a case where the specimen did not suffer localised corrosion, displaying a small hysteresis loop at a high anodic potential. As discussed below, this small hysteresis loop is thought to be due to the depassivation of the specimen surface due to the high potentials reached in the forward PD scan, i.e., the specimen reached the transpassive region [47]. In the first case (Fig. 3a), crevice corrosion was arrested due to repassivation and the term $E_{R,Crev}$ can be used. However, in the example shown in Fig. 3b, the threshold symbolises the transpassive potential (E_{Trans}). Hereafter, to differentiate when the value obtained represented $E_{R,Crev}$ or E_{Trans}, the following criterion was followed. The values obtained were defined as E_{Trans} when the cross-over in the backward PD scan occurred at or above +0.7 $V_{Ag/AgCl}$ (i.e., the drop of potential during the GS step was negligible, resulting in a potential above the reversible potential of the oxygen evolution reaction in the conditions of the test [47]); otherwise, the potential was described as $E_{R,Crev}$.

Fig. 4 illustrates unexpected results of the PD-GS-PD technique. In Fig. 4a, the GS step was triggered due to a metastable attack and high current noise; whereas Fig. 4b shows crevice corrosion starting during the backward PD scan instead of during the GS step. Fig. 5 shows the potential evolution during the GS step for all extruded materials at 50 and 60 °C for both i_{GS} conditions. All forward PD scans reached transpassive potentials, i.e., above the E_{corr} values that could be attained in, e.g., seawater due to the action of microorganisms or chlorination [48].

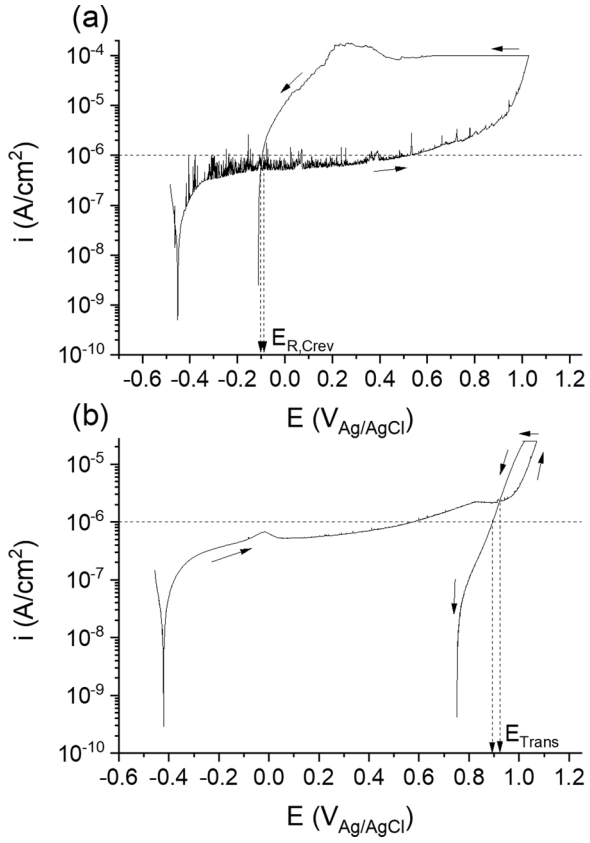

Fig. 3. PD-GS-PD plots of (a) UNS S32750 at 60 °C and (b) UNS S39274 extruded pipe at room temperature. Arrows indicate the direction of the scan. Dashed arrows indicate how $E_{R,Crev}$ and E_{Trans} were obtained from the cross-over potential and 1 μA/cm² definitions.

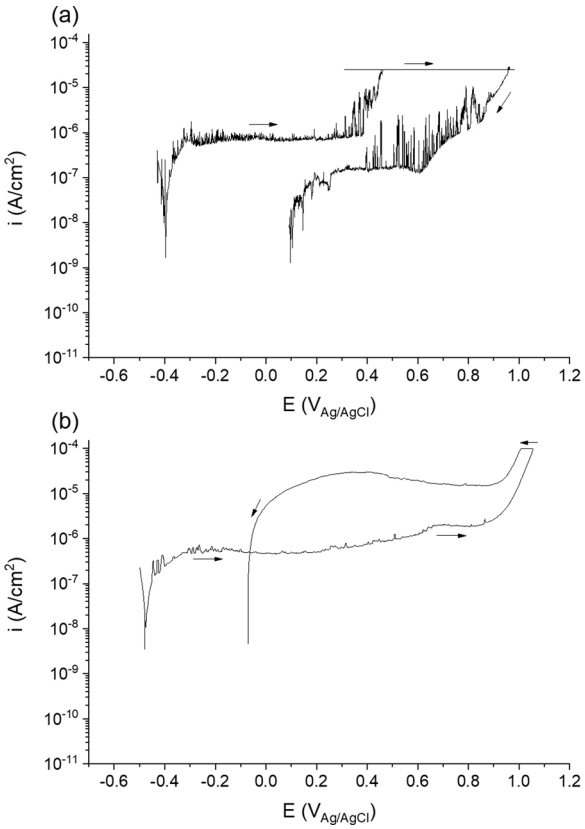

Fig. 4. PD-GS-PD plots of (a) UNS S32760 at 50 °C with an i_{GS} of 25 μA/cm² and (b) UNS S39274 extruded pipe at 60 °C with an i_{GS} of 100 μA/cm². Arrows indicate the direction of the scan.

Nevertheless, apparent metastable activity—evidenced by frequent current spikes—was present in all materials, increasing in intensity at higher temperatures. UNS S32750 and especially UNS S32760 started to show metastable events at room temperature with increasing severity at 40 °C, 50 °C (Fig. 4a), and 60 °C (Fig. 5). On the other hand, UNS S39274 exhibited metastable activity only at temperatures above 50 °C (Fig. 5).

For UNS S32750 and UNS S32760, metastable activity and high current noise reached current densities higher than 25 μA/cm² at 50 °C and 60 °C, causing the GS step of the technique to start at lower potentials. As a result, the potential increased during the GS step as seen in Fig. 5, and the reverse PD scan did not cross the forward PD scan (Fig. 4a), making the determination of $E_{R,Crev}$ impossible. Consequently, the tests at 50 °C and 60 °C were repeated with an i_{GS} of 100 μA/cm². With the higher i_{GS} setting, the forward PD scan continued until reaching a stable critical current. In this regard, the potential during the GS step stayed relatively constant in the absence of crevice attack, while it exhibited a sharp decrease when crevice corrosion initiated, as shown in Fig. 5.

Fig. 6 illustrates the $E_{R,Crev}$ and E_{Trans} for the two i_{GS} values at 50 and 60 °C, whereas Fig. 7 shows $E_{R,Crev}$ and E_{Trans} as function of temperature. The $E_{R,Crev}$ and E_{Trans} values were unaffected by the choice of i_{GS} as shown in Fig. 6. Only for UNS S32760, $E_{R,Crev}$ dropped to +0.15 $V_{Ag/AgCl}$ when using 100 μA/cm², whereas the drop remained at high anodic potentials, i.e., +0.6 $V_{Ag/AgCl}$ with a i_{GS} of 25 μA/cm². Only minor differences were observed in $E_{R,Crev}$ values when comparing the cross over and current criteria, as seen in Fig. 6 and 7. Nevertheless, E_{Trans} obtained with the cross-over definition was slightly more positive than that measured at 1 μA/cm².

Crevice corrosion attack did not occur at room temperature in any of the three SDSS; thus, all the potentials were labelled as E_{Trans}. UNS S32750 transitioned from E_{Trans} to $E_{R,Crev}$ at 40 °C. The transition

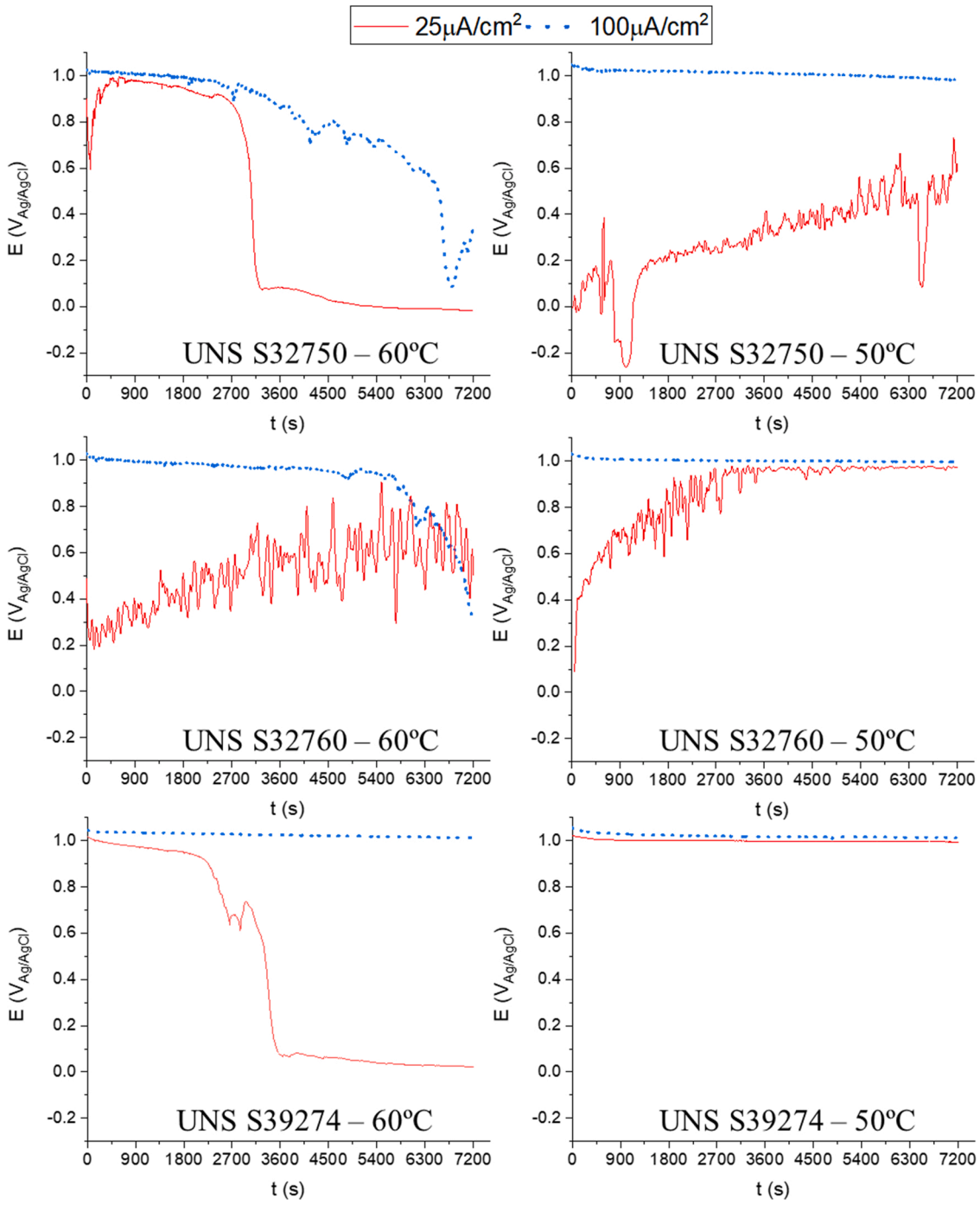

Fig. 5. Potential evolution during the galvanostatic step of the PD-GS-PD tests for the extruded pipe materials tested at 50 °C and 60 °C at two i_{GS} values as indicated.

temperature was 50 °C for UNS S32760 and 60 °C for the UNS S39274 rolled plate. In contrast, UNS S39274 extruded pipe suffered stable crevice corrosion at 60 °C with no clear transition temperature. Despite the absence of a clear transition region (Fig. 6 and 7), the transition temperature was assumed to be between 50 and 60 °C, i.e., approximately 55 °C. At the transition temperature, some specimens showed signs of corrosion while others did not, resulting in a large dispersion in $E_{R,Crev}$ values. Therefore, the minimum number of tests was increased to 8 per condition. Additionally, this large fluctuation suggested that this temperature could be set as $T_{R,Crev}$, since it marked the change from transpassive attack to stable crevice propagation. Table 2 summarises the $T_{R,Crev}$ measured for all the extruded pipe materials.

3.2. Critical crevice and repassivation temperatures in natural seawater

Fig. 8 and Table 2 summarise the results of the long-term natural seawater exposure testing. Figs. 8a and b show OCP and temperature as a function of exposure time, together with an insert presenting a picture of a specimen after the test to illustrate the severity of the crevice corrosion. Figs. 8c and d show the current and temperature evolution for the specimens polarised to +600 $mV_{Ag/AgCl}$, alongside with pictures indicating the extent of crevice corrosion. In the case of UNS S32750 polarized to +600 $mV_{Ag/AgCl}$, the two specimens did not initiate crevice corrosion at the same temperature. Since both specimens were tested simultaneously in the same container, the temperature was increased until the second specimen also developed crevice attack (i.e., specimen 1

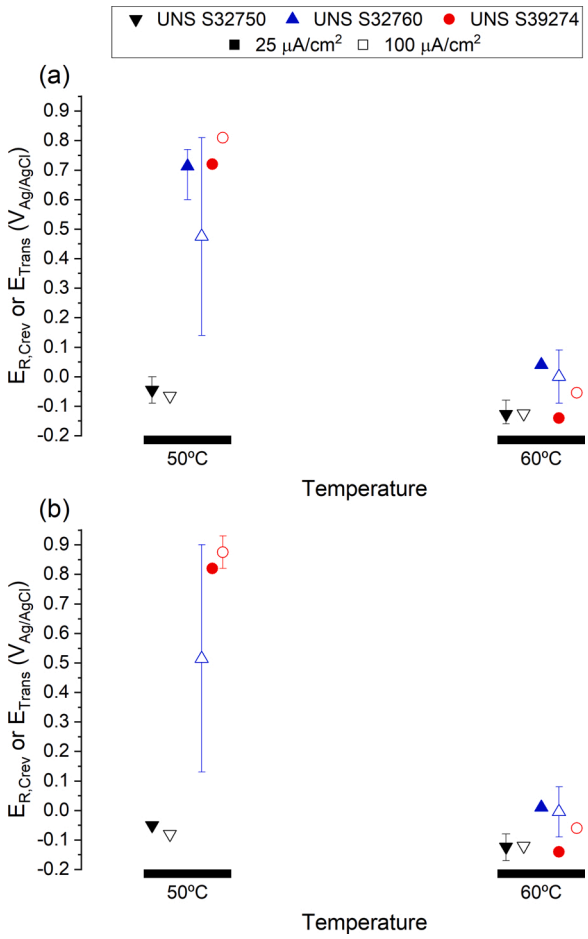

Fig. 6. A comparison of the effect of i_{GS} on $E_{R,Crev}$ and E_{Trans}. The values were obtained for the extruded pipe materials from the PD-GS-PD tests at 50 °C and 60 °C; $E_{R,Crev}$ and E_{Trans} determined as (a) backward PD scan reaching 1 μA/cm^2 and (b) cross-over of forward and backward PD. Error bars show maximum and minimum values.

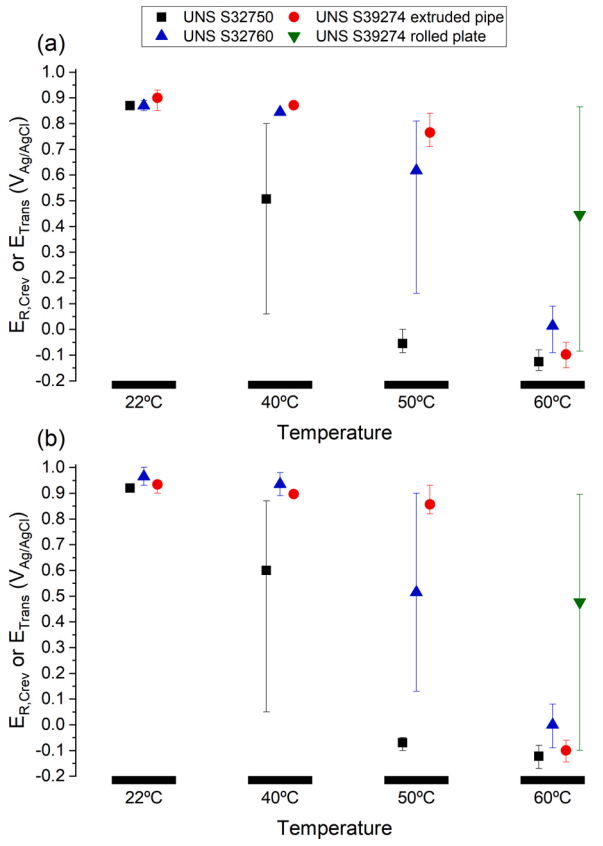

Fig. 7. $E_{R,Crev}$ or E_{Trans} values obtained for all materials from all the PD-GS-PD tests, defined as (a) backward PD scan reaching 1 μA/cm^2, and (b) cross-over of forward and backwards PD. Error bars show maximum and minimum values.

developed crevice at 45 °C while specimen 2 showed crevice corrosion at 50 °C).

As seen in Fig. 8, OCP remained in the 0.05 to 0.25 $V_{Ag/AgCl}$ range in all cases with no clear stepwise drop. At the end of the tests, the external surface was covered by a thin layer of calcareous deposits and only minor signs of attack were found under the crevice formers. In contrast, all specimens polarised at +600 $mV_{Ag/AgCl}$ suffered crevice corrosion. All samples repassivated during the backward temperature stepwise ramp. As seen in Table 2, $T_{R,Crev}$ values were lower than CCT, indicating a hysteresis in critical temperatures. In the particular case of UNS S32750 polarized to +600 $mV_{Ag/AgCl}$, the two specimens obtained different $T_{R,Crev}$ (corresponding to 2.5 °C < CCT, respectively), as indicated in Table 2. UNS S39274 exhibited higher CCT and $T_{R,Crev}$ values than the W-free UNS S32750 (Table 2), suggesting a higher resistance to crevice corrosion.

3.3. Surface characterisation

The number of localised attacks was quantified by visual inspection after both PD-GS-PD and long-term exposure testing. Fig. 9 summarises the total number of localised attacks after PD-GS-PD testing. In this regard, the number of attacks increased with temperature; although UNS S32760 had approximately the same quantity of crevice sites from 40 °C to 60 °C. UNS S39274 had the lowest number of attacks up to 50 °C; while at 60 °C, UNS S32760 and the UNS S32974 rolled plate samples exhibited the lowest number of crevice sites.

Table 2
CCT and $T_{R,Crev}$ values obtained with the PD-GS-PD technique and after long-term exposure in natural seawater for the extruded pipe materials.

UNS	Technique	Potential	CCT (°C)	$T_{R,Crev}$ (°C)
S32750	**PD-GS-PD**		> 60	40
	Natural seawater	**OCP**	> 80	–
		+600 mV$_{Ag/AgCl}$	45 / 50	42.5 / 47.5
S32760	**PD-GS-PD**		> 60	50
	Natural seawater	**OCP**	–	–
		+600 mV$_{Ag/AgCl}$	–	–
S39274	**PD-GS-PD**		> 60	~55
	Natural seawater	**OCP**	> 80	–
		+600 mV$_{Ag/AgCl}$	55	50

Fig. 10 summarises the depth of each attack found on the specimens exposed to natural seawater at OCP, together with the total number of crevice sites, and micrographs of the deepest attack for each material. The average crevice depth was slightly higher in UNS S39274 than in UNS S32750, but in all cases the crevice depth remained below 35 μm. The crevice corrosion severity was drastically higher in the specimens polarised at +600 $mV_{Ag/AgCl}$, where through-thickness penetration of some crevice sites was found, as illustrated in Fig. 8c for UNS S32750. In the case of UNS S39274, the crevice attacks were large, but did not penetrate through the thickness (Fig. 8d).

The extent of all attacks in the PD-GS-PD tests was further quantified and illustrated in Fig. 11 by (a) the total volume of the attack, (b) the projected area on the surface, and (c) the maximum depth of the crevices after PD-GS-PD testing. Some interesting findings can be highlighted by comparing Fig. 11 with the $E_{R,Crev}$ and E_{Trans} extracted from Fig. 7. Below the critical temperature, the extent of transpassive attack was approximately similar in range for the three materials. The dispersion in

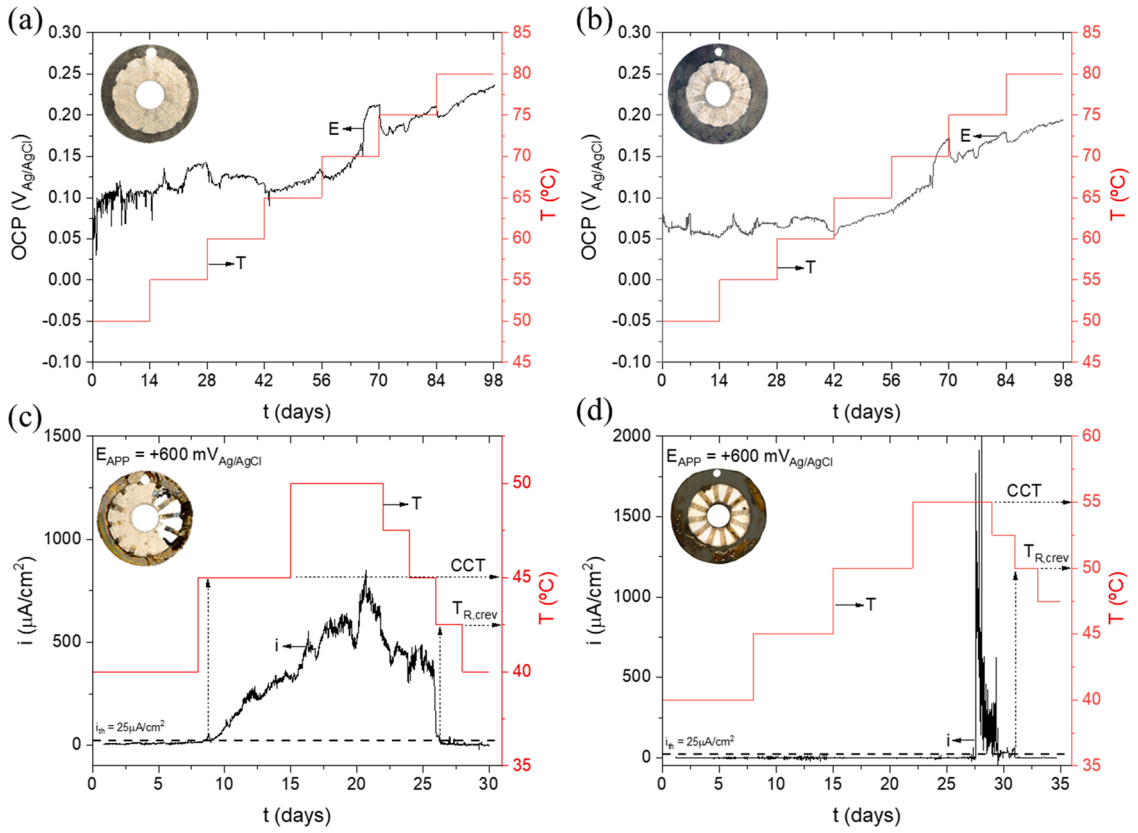

Fig. 8. CCT and $T_{R,Crev}$ tests in natural seawater of extruded pipe materials (a) UNS S32750 at OCP, (b) UNS S39274 at OCP, (c) UNS S32750 polarised to +600 $mV_{Ag/AgCl}$, and (d) UNS S39274 polarised to +600 $mV_{Ag/AgCl}$, the picture inserts show a specimen after exposure to illustrate the attack.

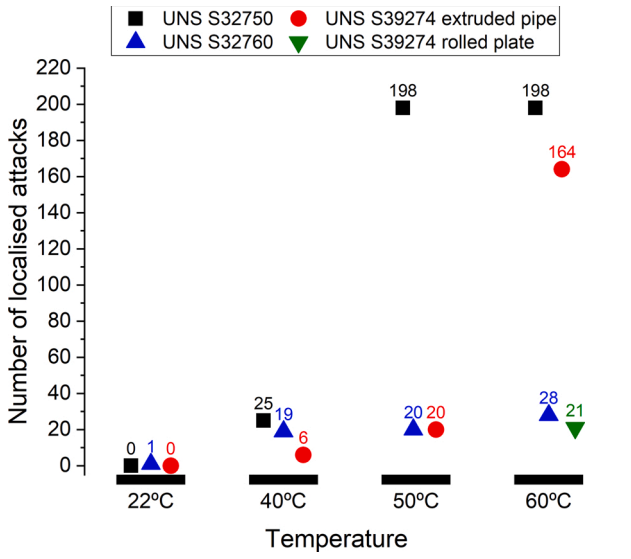

Fig. 9. Total number of localised corrosion attacks in 2 specimens for each material and test temperature after the PD-GS-PD testing.

depth, area, and volume increased as the temperature approached the critical value, with maximum values increasing with temperature for all materials. The large increase in dispersion and the differences in maximum values above and below the $T_{R,Crev}$ can be used to identify the transition from transpassive dissolution to crevice corrosion, as discussed below.

The maximum crevice depth, maximum crevice volume, and maximum corrosion area at the transition between E_{Trans} and $E_{R,Crev}$ were obtained from Fig. 11 and are summarised in Table 3. The maximum crevice depth values gathered in Table 3 were considered the threshold to define the transition to stable crevice attack. Below this value, the attack was considered to be transpassive dissolution. On the contrary, above this value, crevice corrosion took place in the GS or backward PD steps and the potential threshold obtained was $E_{R,Crev}$. Accordingly, crevice corrosion in UNS S32750 stabilised at lower transpassive attack depths than the W-containing SDSS.

Selected samples were further analysed by SEM-EDS to gain a better understanding of the crevice dissolution process. Figs. 12 and 13 illustrate crevice attacks found by SEM after the PD-GS-PD tests. SEM-EDS analysis revealed different degrees of corrosion depending on the propagation size. Selective dissolution of ferrite (α) occurred during the early stages of the attack whereas austenite (γ) corroded as corrosion propagated into the crevice. Thereby, the following 4 stages were identified, and they are numbered in Fig. 12: (i) phase boundary attack, (ii) selective corrosion of α, (iii) initiation of γ dissolution, and (iv) complete dissolution of all phases.

3.4. Additional characterisations

The concentration of ions released after the PD-GS-PD tests was quantified by ICP-MS. Fig. 14 shows the results for the specimens that exhibited crevice corrosion, i.e., low $E_{R,Crev}$ values. For most materials, Cr and Fe cations were the main elements dissolved into the electrolyte. The exception was UNS S39274 rolled plate, which had a preferential W, Ni, and Mo dissolution but a low Cr and Fe release when compared with the other tree materials.

Fig. 15 illustrates the Q_{exp} calculated from the PD-GS-PD tests in C/cm^2, as it is typically reported in the literature. [21,25] The Q_{exp} was four times larger in Fig. 15b than in Fig. 15a because the i_{GS} used was four times higher, as explained in the experimental section. UNS S32750

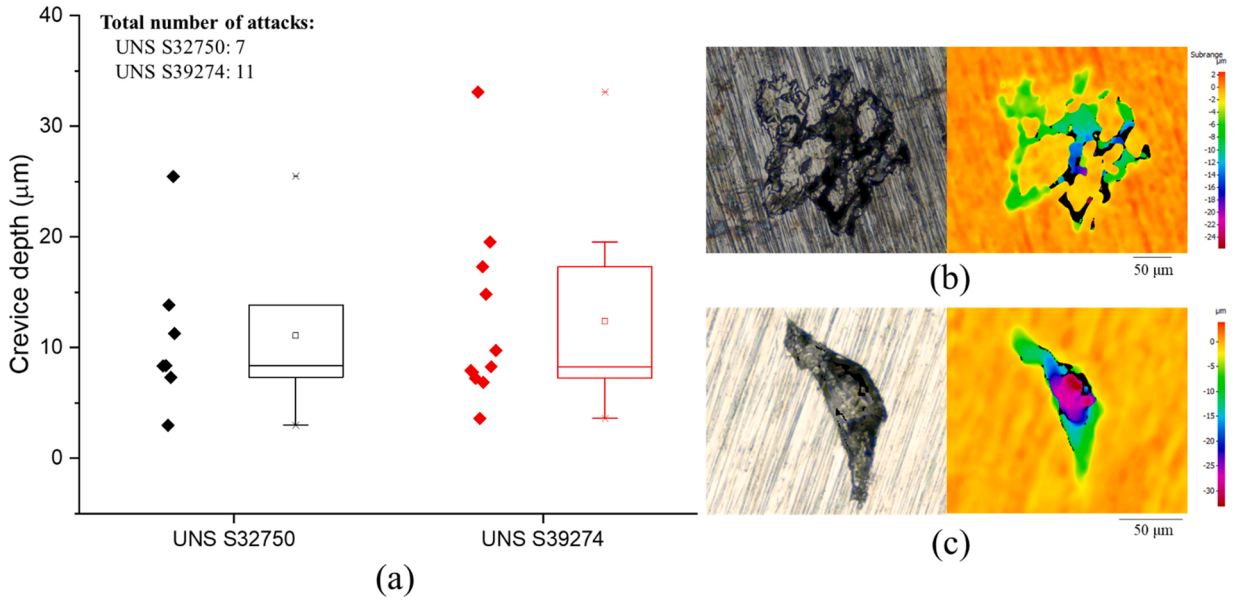

Fig. 10. (a) All localized attacks depths, (b) pictures of deepest attack on UNS S32750, and (c) picture of deepest attack on UNS S39274 found on the specimens exposed at OCP in natural seawater.

had a larger Q_{exp} at 50 °C and the highest Q_{exp} in all cases with an i_{GS} =100 µA/cm^2. Nevertheless, at 60 °C and i_{GS} =25 µA/cm^2, UNS S39274 showed the largest Q_{exp}.

4. Discussion

4.1. Disadvantages of the PD-GS-PD technique

Although the PD-GS-PD technique has been applied successfully to study the crevice corrosion of Ni-alloys [29–35] and some stainless steels [36,37]; in this work, the technique showed limitations. The first issue was the effect of the metastable activity and high current noise experienced for some materials at all temperatures, but particularly near the transition temperature. The current density of these metastable events and the associated current noise was high enough to trigger the GS step before reaching the critical crevice potential or E_{Trans}, as seen in Fig. 4a. As a result, the potential increased during the GS step (Fig. 5) instead of remaining constant (in the case of no corrosion) or decrease with time (if corrosion initiated). Earlier published data [32,35] showed a similar potential increase during the GS step, although it was attributed to the inhibiting effect of Cr or Cu ions in solution being studied and not to an experimental artefact. It was, thus, necessary to increase the value of the i_{GS} from 25 to 100 µA/cm^2 to circumvent this problem. As seen in Fig. 5, the initial potential achieved during the GS step was only slightly higher (approximately 10 mV) with 100 µA/cm^2 than with 25 µA/cm^2.

For samples that developed stable crevice corrosion, the $E_{R,Crev}$ was independent of the choice of i_{GS}, as illustrated in Fig. 6, despite the differences in charge passed during testing (Fig. 15). Even though the Q_{exp} values were lower than those reported for UNS S30400, S31603, and N08825 [21,25], it is, thus, reasonable to assume that the crevices were large enough with both i_{GS} values [30].

The second observation is that, in all cases, the forward scan reached transpassive values, which a priori could influence the crevice initiation step. Even though Cr cannot passivate at transpassive potentials, thermodynamically Fe can [47], and it has been shown that UNS S32750 forms a Fe passive layer at those potentials [49]. Additionally, an insoluble Mo-rich layer has been found at transpassive potentials for Ni-alloys, suggested to form as result of a local decrease in pH due to the hydrolysis of Fe(III) ions dissolved in the crevice solution [50]. Additionally, it has been reported that the passive film on UNS S32750 is completely dissolved at 1.4 $V_{Ag/AgCl}$ [51]. Nevertheless, even if the passive film is not completely dissolved, it is Cr-depleted in comparison with the film at lower passive potentials. As result, the passive film is weaker and transpassive attack can occur [52–54]. Transpassive attack of (S)DSS leads to the preferential attack at phase boundaries [55,56] followed by selective dissolution of the ferrite phase [51,56]. Additionally, Jakobsen et al. [52] found that for temperatures below the CCT, transpassive attack propagates after initiation, but it is unstable.

The presence of a small hysteresis loop even in specimens that did not suffer crevice corrosion (Fig. 3b) is a consequence of reaching transpassive potentials in the forward PD scan. Therefore, the term $E_{R,Crev}$ is not applicable in these situations. Instead, E_{Trans} should be used to indicate that the hysteresis loop was caused by transpassive dissolution. In this work, $E_{R,Crev}$ and E_{Trans} were differentiated based on the E-log(i) behaviour followed by the specimen during the reverse PD scan. In the absence of crevice corrosion, the current density during the reverse PD scan rapidly decreased obtaining a new E_{corr} within the oxygen evolution potential range [47] (Fig. 3b). This E_{corr} coincided with a change in the slope of the forward PD scan, indicating a change in the electrochemical reaction occurring on the surface (most likely signalling the onset of the transpassive region or the oxygen evolution reaction [47]).

Based on the observations presented above, it is, thus, reasonable to assume that crevice corrosion initiation on SDSS during PD-GS-PD testing at temperatures below CCT requires a minimum amount of transpassive attack in the forward PD scan or during the initial stage of the GS step. In this regard, repassivation will occur quickly and at high potentials if the depth of the transpassive attack is below a critical value, $x_{Crit,Trans}$. Contrarily, crevice corrosion will initiate and propagate during the GS and backward PD steps above $x_{Crit,Trans}$. The maximum depth of the transpassive attack found at the transition temperature, i.e., below the $T_{R,Crev}$, was considered as an estimator of $x_{Crit,Trans}$. As seen in Table 3, W increased the maximum depth of the transpassive attack, suggesting an increase in the critical depth required to stabilize crevice corrosion.

Another unexpected result was the delay in the crevice corrosion initiation for some of the specimens. In some instances, crevice corrosion initiated during the backward PD scan, instead of during the GS step as seen in Fig. 4b. The same behaviour was observed in other works [36,44,57] for cases where the material suffered mild localised corrosion. This

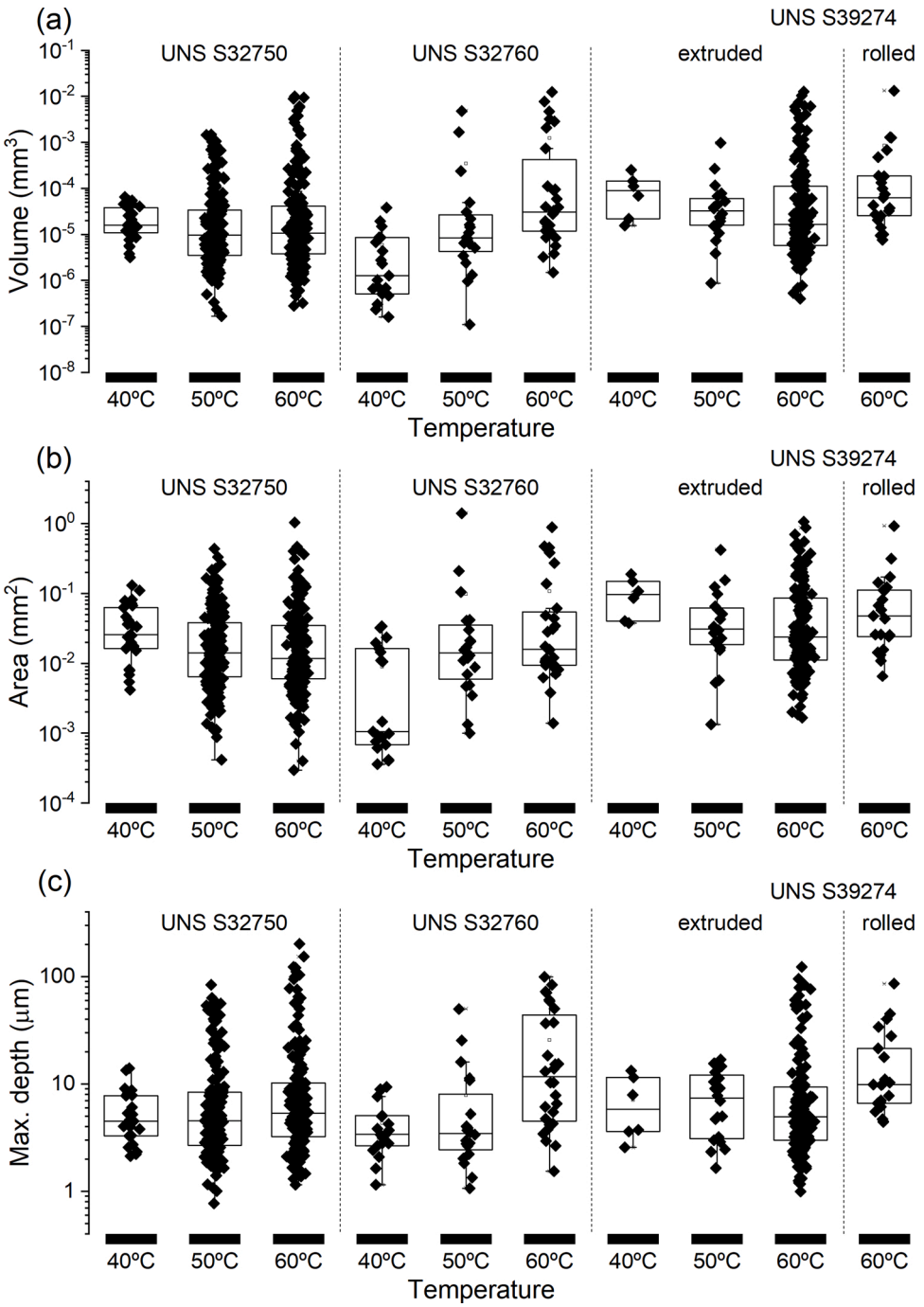

Fig. 11. Crevice size measurements (a) volume, (b) area, and (c) maximum depth present in 2 specimens of all extruded materials after the PD-GS-PD tests at all temperatures.

Table 3
Maximum depth, volume and surface area of transpassive attacks found in each material. The max. depth represents the depth of the transpassive attack at the transition temperature and it was taken as an estimator of $x_{Crit,Trans}$.

Material (UNS)	E_{Trans} ($V_{Ag/AgCl}$)	T (°C)	Max. depth (µm)	Volume (mm^3)	Area (mm^2)
S32750	0.80	40	7.9	$2.86 \cdot 10^{-5}$	0.067
S32760	0.81	50	16.1	$2.40 \cdot 10^{-4}$	0.105
S39274 extruded pipe	0.78	50	16.9	$9.77 \cdot 10^{-4}$	0.421
S39274 rolled plate	0.87	60	45.2	$1.29 \cdot 10^{-3}$	0.172

issue may be avoided by either extending the duration of the GS step, by using PTFE-covered ceramic crevice formers since they have been shown to produce more demanding crevices in highly corrosion resistant nickel-based alloys [31,58,59], or both. Nevertheless, $E_{R,Crev}$ values were independent of whether crevice corrosion started in the GS or backward PD step. The Q_{exp} measured in both cases was similar, suggesting the same extent of the crevice attack.

During the backward PD scan, all specimens experienced a maximum in current density around 0.1 to 0.4 $V_{Ag/AgCl}$ (e.g., Figs. 3a and 4b). In this regard, the reversible potential for the reduction of Cr(VI) to Cr(III) lies within this potential range for the tested conditions [47]. Therefore, the formation of a Cr-rich passive film is thermodynamically stable in this potential range and, consequently, the current density drops shortly

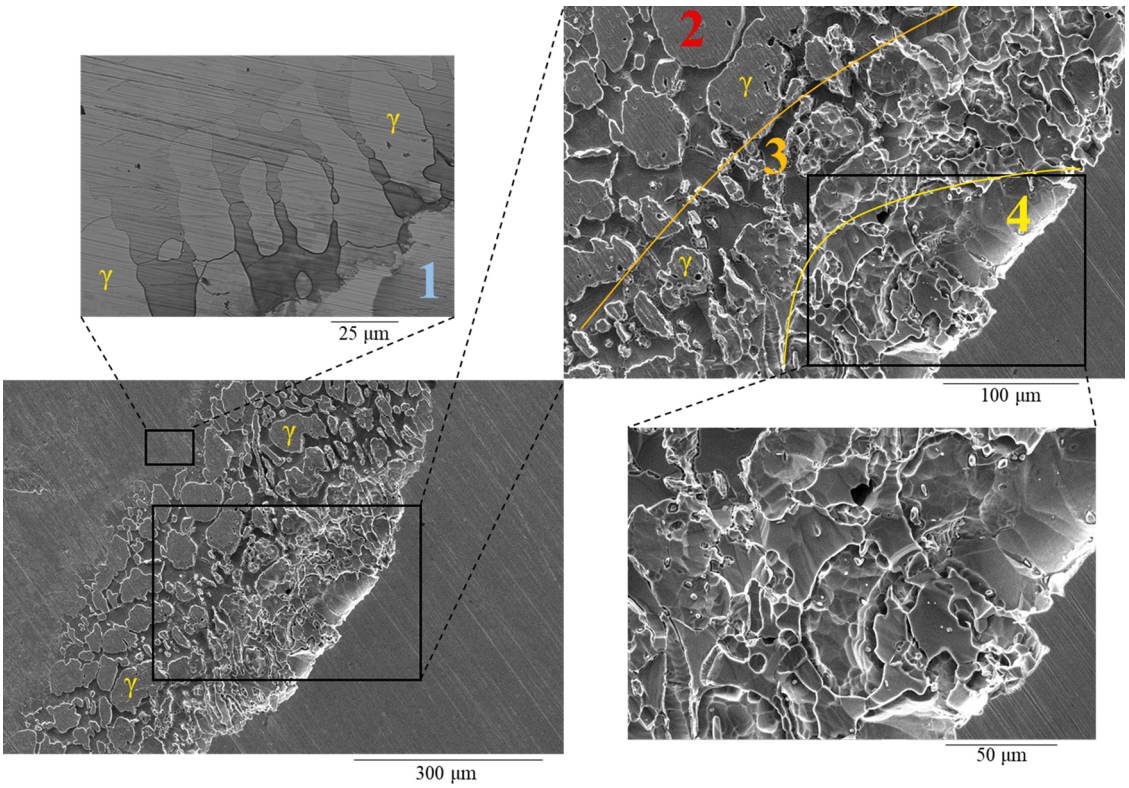

Fig. 12. SEM pictures of a crevice attack found in UNS S32750 after the PD-GS-PD tests at 60 °C. The numbers indicate the propagation stage: (1) phase boundary attack as the attack grows in area, (2) selective dissolution of α phase, (3) partial γ dissolution, and (4) γ is completely dissolved and the attack deepens.

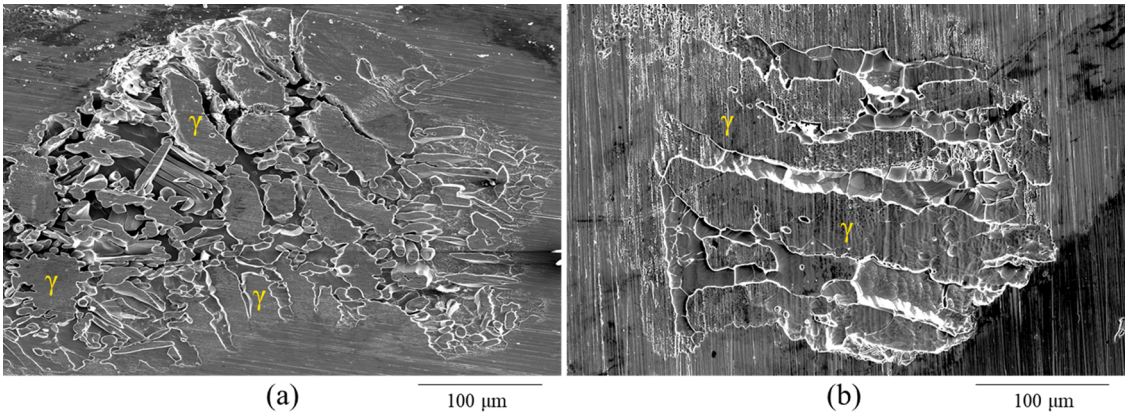

Fig. 13. SEM pictures illustrating the crevice attack found in UNS S39274 (a) extruded pipe and (b) rolled plate after the PD-GS-PD tests at 60 °C.

after, stifling crevice corrosion propagation.

4.2. *Effect of W on crevice corrosion resistance*

Crevice corrosion did not initiate in the forward scan for any of the materials in the tested temperature conditions, making the determination of the CCT impossible. CCT values of UNS S32750 reported in the literature obtained from CPP tests are in the 65-70 °C range both in simulated and natural seawater environments [7,44], which are above the temperatures tested herein. The $T_{R,Crev}$ was determined as the temperature at which the results transitioned from E_{Trans} to $E_{R,Crev}$, as explained in section 3.1. Peguet et al. [55] described a transition temperature interval for CPT up to 10 °C for the DSS UNS S32205. On the other hand, Sun et al. [60] suggested that only DSSs present the transition temperature interval because of their inhomogeneous microstructure, as the austenitic stainless steels tested by these authors showed a sharp CPT transition. Nevertheless, since the temperature interval used herein was ≥ 10 °C, no clear transition temperature interval could be observed for the $T_{R,Crev}$.

The long-term experiments in natural seawater performed in this work showed that specimens freely exposed in natural seawater exhibited small attacks that did not affect the OCP up to 80 °C, which made the determination of the critical temperature impossible. In contrast, the CCT measured at an applied potential of +600 $mV_{Ag/AgCl}$, which simulated chlorination treatments [7,40], was 45 °C and 55 °C for UNS S32750 and UNS S39274, respectively. Interestingly, the CCT values determined from the potentiostatic long-term exposure tests were similar to the $T_{R,Crev}$ results of the PD-GS-PD tests (Table 2), suggesting that, for SDSS, $T_{R,Crev}$ obtained by PD-GS-PD could be used as an estimator of crevice corrosion initiation in materials selection.

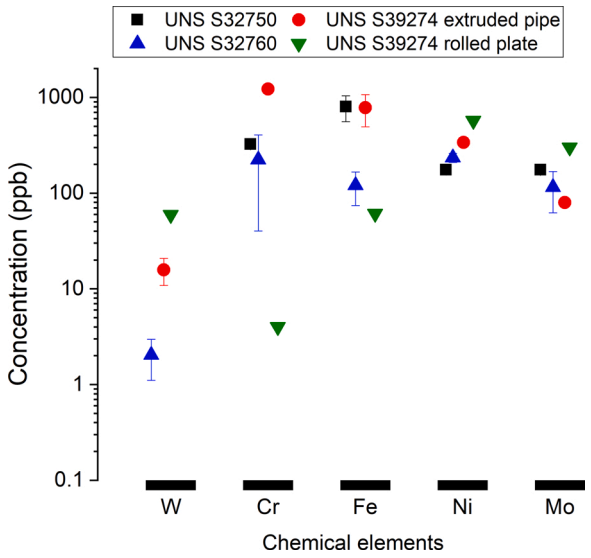

Fig. 14. Concentration of ions released in the electrolyte after the PD-GS-PD tests at 60 °C. Due to the logarithm scale of the concentration axis, error bars are not visible.

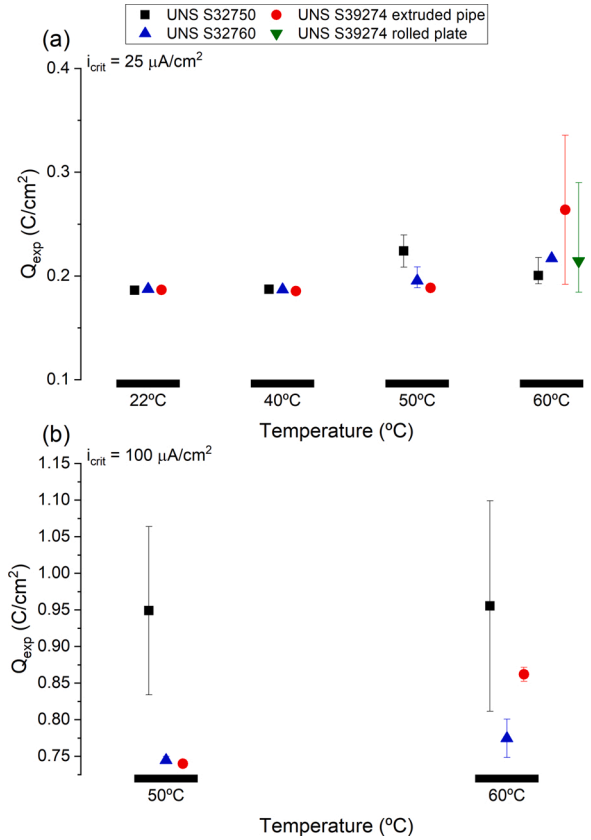

Fig. 15. Q_{exp} calculated from the GS step and the reverse PD scan for all materials tested at (a) i_{GS} =25 μA/cm², and (b) i_{GS} =100 μA/cm². Error bars show maximum and minimum values.

The $T_{R,Crev}$ of UNS S32750 obtained by PD-GS-PD testing and after long-term exposure (i.e., 40 and 42.4 °C, respectively) was lower than reported values in natural or simulated seawater environments (i.e., 56 °C) [7,44]. The differences in $T_{R,Crev}$ were attributed to the severity of the PD-GS-PD technique when compared to the CPP method and the extended duration of the temperature steps in the long-term test. Only one study [36] obtained a lower $T_{R,Crev}$ than in this work – the $T_{R,Crev}$ was below 30 °C-, even though the electrolyte consisted of a more dilute NaCl solution (10,000 ppm Cl^-). The same PD-GS-PD technique was used, but the crevice formers were ceramic and covered with PTFE tape, resulting in a more aggressive localised attack [31,58,59].

Despite the experimental limitations discussed above, results indicated that tungsten increased the crevice corrosion resistance of SDSS, as determined by both CCT and $T_{R,Crev}$ values (Figs. 7 and 8 and Table 2), and indirectly by the increase in $x_{Crit,Trans}$ (Table 3). In this regard, the W-free material (UNS S32750) had the lowest $T_{R,Crev}$ measured both by the PD-GS-PD method and potentiostatic testing at +600 $mV_{Ag/AgCl}$ in natural seawater (i.e., 40 and 42.5 °C, respectively), whereas $T_{R,Crev}$ increased with incremental W content as summarised in Table 2. These findings are in agreement with a previous work [7] where only two SDSSs containing different degrees of W were investigated by performing CPP. By including a W-free SDSS as a reference, the enhancement of localized corrosion resistance due to the W could be inferred. Additionally, a higher extent of crevice corrosion propagation was achieved by using the PD-GS-PD technique in comparison to the CPP, facilitating a better comparison among the materials in a wider temperature range.

It might be questioned, however, whether the small changes in the concentration of other alloying elements as seen in Table 1 could explain the differences observed in this investigation. In this regard, some of the elements have an important weight in the PRE formula such as Cr, Mo and N. Nevertheless, the impact of such changes in composition could be ruled out by comparing $T_{R,Crev}$ values of the different SDSS. In this regard, the W-free UNS S32750 contained the highest amount of Cr and Mo, yet showed the lowest $T_{R,Crev}$ values. Similarly, UNS S32760 contained the lowest amount of N among the SDSSs but gave an intermediate $T_{R,Crev}$ result. Another element—not included in the standard PRE expression—that has been shown to increase the CPT and the overall localized corrosion resistance in halide environments is Cu [61,62]. However, as discussed by Haugan et al. [7] the improvement in CPT in DSS by Cu was much lower than that obtained by W, and, thus, the role of small changes in Cu content could be ignored.

4.3. *Influence of the manufacturing route*

Haugan et al. [7], investigated the effect of W on the crevice corrosion resistance of two SDSS using a combination of methods that included CPP testing. However, the two SDSS studied also differed in product form. In this regard, the high-W UNS S32974 was produced as a rolled plate, whereas the UNS S32750 samples were extracted from an extruded pipe. Given that product form-to-product form variations can have an important effect on localised corrosion resistance [63], the influence of the manufacturing route was also studied herein, using samples extracted from the same plate as Haugan et al. [7].

As seen in Table 1, the rolled plate specimens had a higher Ni and N content than the extruded pipe specimens. Conversely, the Mo, Cu, and Fe contents were slightly lower in the rolled plate. Even though Ni improves the corrosion resistance in acidic reducing environments, it does not influence localised corrosion resistance in oxidising chloride-containing solutions [3]. Despite the differences in N and Mo content, both materials had identical PRE values. Consequently, based on their chemical composition both materials were expected to exhibit similar crevice corrosion resistance. However, the results in this work (Fig. 7) showed a small but measurable influence of the manufacturing process in the $T_{R,Crev}$ values. In this regard, the average $T_{R,Crev}$ of the extruded pipe was approximately 55 °C whereas that of the rolled plate was 60 °C. Additionally, the number of crevice sites (Fig. 9) was higher in the extruded pipe, but the maximum crevice volume was larger in the rolled plate case (Fig. 10). More research is needed to elucidate the influence of product form and heat-to-heat variations on crevice corrosion resistance.

5. Conclusions

In this work, the $T_{R,Crev}$ of three commercial SDSS containing incremental amounts of W was obtained by evaluating the $E_{R,Crev}$ values extracted from PD-GS-PD tests at different temperatures. Results were validated using long-term exposure in natural seawater at both the OCP and potentiostatically at +600 $mV_{Ag/AgCl}$, which allowed the estimation of CCT and $T_{R,Crev}$. The following conclusion were drawn based on the evidence provided in this work:

- The $T_{R,Crev}$ measured by the PD-GS-PD method increased with W content in solid solution.
- The 2.1 wt% UNS S39274 SDSS had the highest $T_{R,Crev}$ and the best crevice corrosion resistance as determined by both PD-GS-PD testing and long-term exposure to natural seawater. In this regard, the CCT and $T_{R,Crev}$ of UNS S39274 were 7.5–15 °C higher than the W-free control, depending on the measurement technique.
- A hysteresis in temperature was observed in the long-term potentiostatic tests at +600 $mV_{Ag/AgCl}$, indicating a difference between CCT and $T_{R,Crev}$ of 2.5. to 5 °C depending on the material.
- The product form of UNS S39274 influenced corrosion resistance, with the rolled plate samples exhibiting a slightly better performance as determined by $T_{R,Crev}$.
- The crevice attack initiated at α/γ boundaries. In all cases, α selectively corroded; whereas dissolution of γ occurred at a later stage during crevice propagation.

Data availability

The raw/processed data generated in this work are available upon request from the corresponding author.

Declaration of Competing Interest

The authors report no declarations of interest.

Acknowledgments

The authors thank Dr. Edgar Hornus (Curtin University) for his contribution to the discussion of the results, and Dr. Syverin Lierhagen (NTNU) for performing the ICP-MS tests in the Department of Chemistry at NTNU. The authors also acknowledge Sumitomo Co. and Sandvik AS, who donated the various materials. This work was sponsored by NTNU's Department of Mechanical and Industrial Engineering.

References

[1] J.M. Kolotyrkin, Pitting corrosion of metals, Corros. 19 (1963), https://doi.org/10.5006/0010-9312-19.8.261, 261t-268t.
[2] A.J. Sedriks, Plenary lecture—1986: effects of alloy composition and microstructure on the passivity of stainless steels, Corros. 42 (1986) 376–389, https://doi.org/10.5006/1.3584918.
[3] C.O.A. Olsson, D. Landolt, Passive films on stainless steels—chemistry, structure and growth, Electrochim. Acta 48 (2003) 1093–1104, https://doi.org/10.1016/s0013-4686(02)00841-1.
[4] R.C. Newman, W.R. Whitney award lecture: understanding the corrosion of stainless steel, Corros. 57 (2001) (2001) 1030–1041, https://doi.org/10.5006/1.3281676.
[5] J.O. Nilsson, Super duplex stainless steels, Mater. Sci. Technol. 8 (1992) 685–700, https://doi.org/10.1179/mst.1992.8.8.685.
[6] R.F.A. Jargelius-Pettersson, Application of the pitting resistance equivalent concept to some highly alloyed austenitic stainless steels, Corros. 54 (1998) 162–168, https://doi.org/10.5006/1.3284840.
[7] E.B. Haugan, M. Næss, C. Torres Rodriguez, R. Johnsen, M. Iannuzzi, Effect of tungsten on the pitting and crevice corrosion resistance of type 25Cr super duplex stainless steels, Corros. 73 (2017) 53–67, https://doi.org/10.5006/2185.
[8] C. Torres, M.S. Hazarabedian, Z. Quadir, R. Johnsen, M. Iannuzzi, The role of tungsten on the phase transformation kinetics and its correlation with the localized corrosion resistance of 25Cr super duplex stainless steels, J. Electrochem. Soc. 167 (2020), https://doi.org/10.1149/1945-7111/ab90af, 081510.
[9] N. Bui, A. Irhzo, F. Dabosi, Y. Limouzin-Maire, On the mechanism for improved passivation by additions of tungsten to austenitic stainless steels, Corros. 39 (1983) 491–496, https://doi.org/10.5006/1.3577373.
[10] A. Belfrouh, C. Masson, D. Vouagner, A.M. de Becdelievre, N.S. Prakash, J. P. Audouard, The cumulative effect of alloying elements N, W, Mo and Cu on the corrosion behaviour of 17Cr-13Ni stainless steel in 2 N H2SO4, Corros. Sci. 38 (1996) 1639–1648, https://doi.org/10.1016/s0010-938x(96)00033-9.
[11] N.D. Tomashov, G.P. Chernova, O.N. Marcova, Effect of supplementary alloying elements on pitting corrosion susceptibility of 18Cr-14Ni stainless steel, Corros. 20 (1964), https://doi.org/10.5006/0010-9312-20.5.166t, 166t-173t.
[12] M.K. Ahn, H.S. Kwon, H.M. Lee, Quantitative comparison of the influences of tungsten and molybdenum on the passivity of Fe-29Cr ferritic stainless steels, Corros. Sci. 40 (1998) 307–322, https://doi.org/10.1016/s0010-938x(97)00138-8.
[13] E.-A. Cho, C.-K. Kim, J.-S. Kim, H.-S. Kwon, Quantitative analysis of repassivation kinetics of ferritic stainless steels based on the high field ion conduction model, Electrochim. Acta 45 (2000) 1933–1942, https://doi.org/10.1016/s0013-4686(99)00415-6.
[14] R. Goetz, J. Laurent, D. Landolt, The influence of minor alloying elements on the passivation behaviour of iron-chromium alloys in HCl, Corros. Sci. 25 (1985) 1115–1126, https://doi.org/10.1016/0010-938x(85)90057-5.
[15] H. Habazaki, A. Kawashima, K. Asami, K. Hashimoto, The corrosion behavior of amorphous Fe-Cr-Mo-P-C and Fe-Cr-W-P-C alloys in 6 M HCl solution, Corros. Sci. 33 (1992) 225–236, https://doi.org/10.1016/0010-938x(92)90147-u.
[16] ASTM International, Standard Test Method for Conducting Cyclic Potentiodynamic Polarization Measurements for Localized Corrosion Susceptibility of Iron-, Nickel-, or Cobalt-Based Alloys, in, West Conshohocken, PA, 2018, DOI: 10.1520/G0061-86R18.
[17] R.M. Carranza, Environmental and Metallurgical Variables Affecting Crevice Corrosion Susceptibility of Alloy 22 - a Review, in: Corrosion 2008, NACE International, 2008, p. 16.
[18] I.L. Rosenfeld, Breakdown of the passive state and repassivation of stainless steels, J. Electrochem. Soc. 125 (1978) 1729–1735, https://doi.org/10.1149/1.2131284.
[19] R.C. Newman, E.M. Franz, Growth and repassivation of single corrosion pits in stainless steel, Corros. 40 (1984) 325–330, https://doi.org/10.5006/1.3593930.
[20] N.G. Thompson, B.C. Syrett, Relationship between conventional pitting and protection potentials and a new, unique pitting potential, Corros. 48 (1992) 649–659, https://doi.org/10.5006/1.3315985.
[21] D.S. Dunn, G.A. Cragnolino, N. Sridhar, An electrochemical approach to predicting long-term localized corrosion of corrosion-resistant high-level waste container materials, Corros. 56 (2000) 90–104, https://doi.org/10.5006/1.3280526.
[22] T. Nakayama, K. Sasa, Effect of ultrasonic waves on the pitting potentials of 18-8 stainless steel in sodium chloride solution, Corros. 32 (1976) 283–285, https://doi.org/10.5006/0010-9312-32.7.283.
[23] H. Yashiro, K. Tanno, The effect of electrolyte composition on the pitting and repassivation behavior of AISI 304 stainless steel at high temperature, Corros. Sci. 31 (1990) 485–490, https://doi.org/10.1016/0010-938x(90)90150-4.
[24] E.C. Hornus, M.A. Rodríguez, R.M. Carranza, R.B. Rebak, Effect of temperature and chloride concentration on the crevice corrosion resistance of austenitic stainless steels. Corrosion 2016, NACE International, 2016.
[25] N. Sridhar, G.A. Cragnolino, Applicability of repassivation potential for long-term prediction of localized corrosion of alloy 825 and type 316L stainless steel, Corros. 49 (1993) 885–894, https://doi.org/10.5006/1.3316014.
[26] T. Shibata, T. Takeyama, Stochastic theory of pitting corrosion, Corros. 33 (1977) 243–251, https://doi.org/10.5006/0010-9312-33.7.243.
[27] S. Tsujikawa, Y. Hisamatsu, On the repassivation potential for crevice corrosion, Corros. Eng. 29 (1980) 37–40, https://doi.org/10.3323/jcorr1974.29.1_37.
[28] ASTM International, Standard Test Method for Determining the Crevice Repassivation Potential of Corrosion-Resistant Alloys Using a Potentiodynamic-Galvanostatic-Potentiostatic Technique, in, ASTM International, West Conshohocken, PA, 2014, DOI: 10.1520/G0192-08R14.
[29] A.K. Mishra, G.S. Frankel, Crevice corrosion repassivation of alloy 22 in aggressive environments, Corros. 64 (2008) 836–844, https://doi.org/10.5006/1.3279917.
[30] M.R. Ortíz, M.A. Rodríguez, R.M. Carranza, R.B. Rebak, Determination of the crevice corrosion stabilization and repassivation potentials of a corrosion-resistant alloy, Corros. 66 (2010), https://doi.org/10.5006/1.3500830, 105002-105002-105012.
[31] C.M. Giordano, M. Rincón Ortíz, M.A. Rodríguez, R.M. Carranza, R.B. Rebak, Crevice corrosion testing methods for measuring repassivation potential of alloy 22, Corros. Eng. Sci. Technol. 46 (2011) 129–133, https://doi.org/10.1179/1743278210y.0000000014.
[32] M. Rincón Ortíz, M.A. Rodríguez, R.M. Carranza, R.B. Rebak, Oxyanions as inhibitors of chloride-induced crevice corrosion of Alloy 22, Corros. Sci. 68 (2013) 72–83, https://doi.org/10.1016/j.corsci.2012.10.037.
[33] A.K. Mishra, D.W. Shoesmith, Effect of alloying elements on crevice corrosion inhibition of nickel-chromium-Molybdenum-Tungsten alloys under aggressive conditions: an electrochemical study, Corros. 70 (2014) 721–730, https://doi.org/10.5006/1170.
[34] E.C. Hornus, C.M. Giordano, M.A. Rodriguez, R.M. Carranza, R.B. Rebak, Effect of temperature on the crevice corrosion of nickel alloys containing chromium and molybdenum, J. Electrochem. Soc. 162 (2015) C105–C113, https://doi.org/10.1149/2.0431503jes.
[35] A.K. Mishra, X. Zhang, D.W. Shoesmith, The role of copper on the crevice corrosion behavior of nickel-chromium-Molybdenum alloys in aggressive solutions, Corros. 72 (2016) 356–367, https://doi.org/10.5006/1876.

[36] P.A. Martínez, E.C. Hornus, M.A. Rodríguez, R.M. Carranza, R.B. Rebak, Crevice corrosion resistance of super-austenitic and super-duplex stainless steels in chloride solutions. Corrosion 2015, NACE International, Dallas, Texas, 2015.
[37] M.A. Kappes, M.R. Ortíz, M. Iannuzzi, R.M. Carranza, Use of the critical acidification model to estimate critical localized corrosion potentials of duplex stainless steels, Corros. 73 (2017) 31–40, https://doi.org/10.5006/2142.
[38] E.A. Abd El Meguid, A.A. Abd El Latif, Electrochemical and SEM study on Type 254 SMO stainless steel in chloride solutions, Corros. Sci. 46 (2004) 2431–2444, https://doi.org/10.1016/j.corsci.2004.01.022.
[39] ISO, Corrosion of metals and alloys - Crevice corrosion formers with disc springs for flat specimens or tubes made from stainless steel, in, International Organization for Standardization, Geneva, Switzerland, 2015.
[40] R. Johnsen, H. Vingsand, Corrosion Properties Of UNS S32750, UNS N06022 And UNS N10276 In Seawater. Corrosion 2009, NACE International, 2009, 09195.
[41] S. Valen, P.O. Gartland, Crevice corrosion repassivation temperatures of highly alloyed stainless steels, Corros. 51 (1995) 750–756, https://doi.org/10.5006/1.3293552.
[42] U. Steinsmo, T. Rogne, J.M. Drugli, P.O. Gartland, Critical crevice temperature for high-alloyed stainless steels in chlorinated seawater applications, Corros. 53 (1997) 26–32, https://doi.org/10.5006/1.3280430.
[43] A.B. Høydal, E. Skavås, T. Hemmingsen, crevice corrosion on super duplex stainless steel – effect of potential on critical crevice corrosion temperature. Corrosion 2013, NACE International, 2013.
[44] L.L. Machuca, S.I. Bailey, R. Gubner, Systematic study of the corrosion properties of selected high-resistance alloys in natural seawater, Corros. Sci. 64 (2012) 8–16, https://doi.org/10.1016/j.corsci.2012.06.029.
[45] J.W. Oldfield, W.H. Sutton, Crevice corrosion of stainless steels: II. Experimental studies, Br. Corros. J. 13 (1978) 104–111, https://doi.org/10.1179/000705978798276258.
[46] Digital Surf, www.digitalsurf.com, 1996 (accessed 14 February 2020).
[47] M. Pourbaix, Atlas of Electrochemical Equilibria in Aqueous Solutions, National Association of Corrosion Engineers (NACE), Houston, Texas, USA, 1974.
[48] E. Bardal, J.M. Drugli, P.O. Gartland, The behaviour of corrosion-resistant steels in seawater: a review, Corros. Sci. 35 (1993) 257–267, https://doi.org/10.1016/0010-938x(93)90157-c.
[49] G. Tranchida, F. Di Franco, M. Santamaria, Role of molybdenum on the electronic properties of passive films on stainless steels, J. Electrochem. Soc. 167 (2020), https://doi.org/10.1149/1945-7111/ab7f8a.
[50] J.D. Henderson, X. Li, D.W. Shoesmith, J.J. Noël, K. Ogle, Molybdenum surface enrichment and release during transpassive dissolution of Ni-based alloys, Corros. Sci. 147 (2019) 32–40, https://doi.org/10.1016/j.corsci.2018.11.005.
[51] C. Örnek, M. Långberg, J. Evertsson, G. Harlow, W. Linpé, L. Rullik, F. Carlà, R. Felici, E. Bettini, U. Kivisäkk, E. Lundgren, J. Pan, In-situ synchrotron GIXRD study of passive film evolution on duplex stainless steel in corrosive environment, Corros. Sci. 141 (2018) 18–21, https://doi.org/10.1016/j.corsci.2018.06.040.
[52] P.T. Jakobsen, E. Maahn, Temperature and potential dependence of crevice corrosion of AISI 316 stainless steel, Corros. Sci. 43 (2001) 1693–1709, https://doi.org/10.1016/s0010-938x(00)00167-0.
[53] I. Betova, M. Bojinov, T. Laitinen, K. Mäkelä, P. Pohjanne, T. Saario, The transpassive dissolution mechanism of highly alloyed stainless steels, Corros. Sci. 44 (2002) 2675–2697, https://doi.org/10.1016/s0010-938x(02)00073-2.
[54] G. Song, Transpassivation of Fe–Cr–Ni stainless steels, Corros. Sci. 47 (2005) 1953–1987, https://doi.org/10.1016/j.corsci.2004.09.007.
[55] L. Peguet, A. Gaugain, C. Dussart, B. Malki, B. Baroux, Statistical study of the critical pitting temperature of 22-05 duplex stainless steel, Corros. Sci. 60 (2012) 280–283, https://doi.org/10.1016/j.corsci.2012.03.025.
[56] L. Peguet, A. Gaugain, Localized corrosion resistance of duplex stainless steels: methodology and properties; a review paper, Rev. Mã©tallurgie 108 (2011) 231–243, https://doi.org/10.1051/metal/2011062.
[57] G. Mori, D. Bauernfeind, Pitting and crevice corrosion of superaustenitic stainless steels, Mater. Corros. 55 (2004) 164–173, https://doi.org/10.1002/maco.200303746.
[58] X. Shan, J.H. Payer, Comparison of ceramic and polymer crevice formers on the crevice corrosion behavior of Ni-Cr-Mo alloy C-22. Corrosion 2007, NACE International, 2007.
[59] X. Shan, J.H. Payer, Effect of polymer and ceramic crevice formers on the crevice corrosion of Ni-Cr-Mo alloy 22, Corros. 66 (2010), https://doi.org/10.5006/1.3500833, 105005-105005-105014.
[60] Y.T. Sun, J.M. Wang, Y.M. Jiang, J. Li, A comparative study on potentiodynamic and potentiostatic critical pitting temperature of austenitic stainless steels, Mater. Corros. 69 (2018) 44–52, https://doi.org/10.1002/maco.201709641.
[61] L.F. Garfias-Mesias, J.M. Sykes, C.D.S. Tuck, The effect of phase compositions on the pitting corrosion of 25 Cr duplex stainless steel in chloride solutions, Corros. Sci. 38 (1996) 1319–1330, https://doi.org/10.1016/0010-938x(96)00022-4.
[62] L.F. Garfias-Mesias, J.M. Sykes, Effect of copper on active dissolution and pitting corrosion of 25% Cr duplex stainless steels, Corros. 54 (1998) 40–47, https://doi.org/10.5006/1.3284827.
[63] F. Bocher, R. Huang, J.R. Scully, Prediction of critical crevice potentials for Ni-Cr-Mo alloys in simulated crevice solutions as a function of molybdenum content, Corros. 66 (2010), https://doi.org/10.5006/1.3430462, 055002-055001 to 055002-055015.